

Electrochemical Shot Noise of a Redox Monolayer

Simon Grall, Shuo Li, Laurent Jalabert, Soo-Hyeon Kim and Nicolas Clément*

IIS, LIMMS/CNRS-IIS IRL2820, The Univ. of Tokyo; 4-6-1 Komaba, Meguro-ku Tokyo, 153-8505, Japan

Arnaud Chovin, Christophe Demaille†

Université Paris Cité, CNRS, Laboratoire d'Electrochimie Moléculaire, F-75013 Paris, France

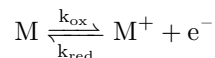
(Dated: March 6, 2023)

Redox monolayers are the base for a wide variety of devices including high-frequency molecular diodes or biomolecular sensors. We introduce a formalism to describe the electrochemical shot noise of such monolayer, confirmed experimentally at room temperature in liquid. The proposed method, carried out at equilibrium, avoids parasitic capacitance, increases the sensitivity and allows to obtain quantitative information such as the electronic coupling (or standard electron transfer rates), its dispersion and the number of molecules. Unlike in solid-state physics, the homogeneity in energy levels and transfer rates in the monolayer yields a Lorentzian spectrum. This first step for shot noise studies in molecular electrochemical systems opens perspectives for quantum transport studies in liquid environment at room temperature as well as highly sensitive measurements for bioelectrochemical sensors.

Self-assembled monolayers (SAM) composed of nanometric-long redox molecules are building blocks for molecular electronics and electrochemistry. They can behave as molecular diodes operating at ultra-high-frequency (potentially as rectenna in the visible spectrum) [1, 2], with on-off ratio breaking the Landauer limit [3, 4], and show interesting features such as signatures of collective quantum interference effects at room temperature [5–7]. In addition, their operation in liquid offers a direct link between quantum transport and electrochemistry [8–10] that provides unique opportunities. For example, the nanoscale measurements of electrochemical signals remains extremely challenging while key to the development of nanobiosensors [11]. Several approaches have been explored to tackle the challenge, using redox cycling [12], high frequency measurements [13] and fluorescence [14]. The underlying challenges rise from the presence of parasitic capacitances and from the fact that under typical measurements conditions, the current scales with the sensor area, leading to difficulties in retrieving the signal with micro- and nanoscale electrodes. Simultaneously, these systems offer unique properties as quantum devices. Probably the most intriguing aspect for the solid-state physics community is the potential for millions of single-energy level quantum dots simultaneously operating at room temperature, with extremely small dispersion, tunable electronic coupling [15] and Frank Condon effect [16]. We propose here to exploit and formalize the shot noise induced by reversible single electron transfers of electroactive molecules attached to an electrode as a new, very sensitive electrochemical technique and as a way to characterize the homogeneity in the electronic

properties of these assembled molecular quantum dots. shot noise has been extensively studied in solid-state physics [17] and more recently in molecular electronics [18, 19], but not in electrochemistry, except for the shot noise due to a variation of the number of molecules in a nanogap [20–23]. Such measurements are usually challenging because of the ubiquitous $1/f$ noise (e.g. in solid-state physics [24], quantum transport [25], molecular electronics [26] or in liquid [27]) which is typically circumvented by low-temperature measurements and by measurements at higher relative frequencies. The $1/f$ noise is here not dominant thanks to the well-defined energy level and electron transfer rates of the redox molecules of the monolayer, allowing to study its low-frequency shot noise arising from the sum of single-electrons trapping/detrapping events to each molecule with a narrow distribution in time constants. A simple and straight-forward equation of the shot noise is proposed, giving direct access to the distribution of the charge transfer rates and the number of charge carriers. This approach provides clearly readable signals even when faradaic currents become unmeasurable, avoids the parasitic capacitance issue and allows for measurements without extra excitation other than the thermal noise.

Electroactive redox molecules can be seen as single-electron quantum dots with extremely small energy dispersion, even in liquid and at ambient temperature [5]. The equilibrium reaction of an ideally reversible redox couple M^+/M attached to a metallic electrode and held at a distance z from the electrode (insets Figure 1 (a)) can be written as:



Using the Marcus-Hush formalism to describe the electron transfer rates gives [28]:

* Nicolas Clément: nclement@iis.u-tokyo.ac.jp

† Christophe Demaille: christophe.demaille@univ-paris-diderot.fr

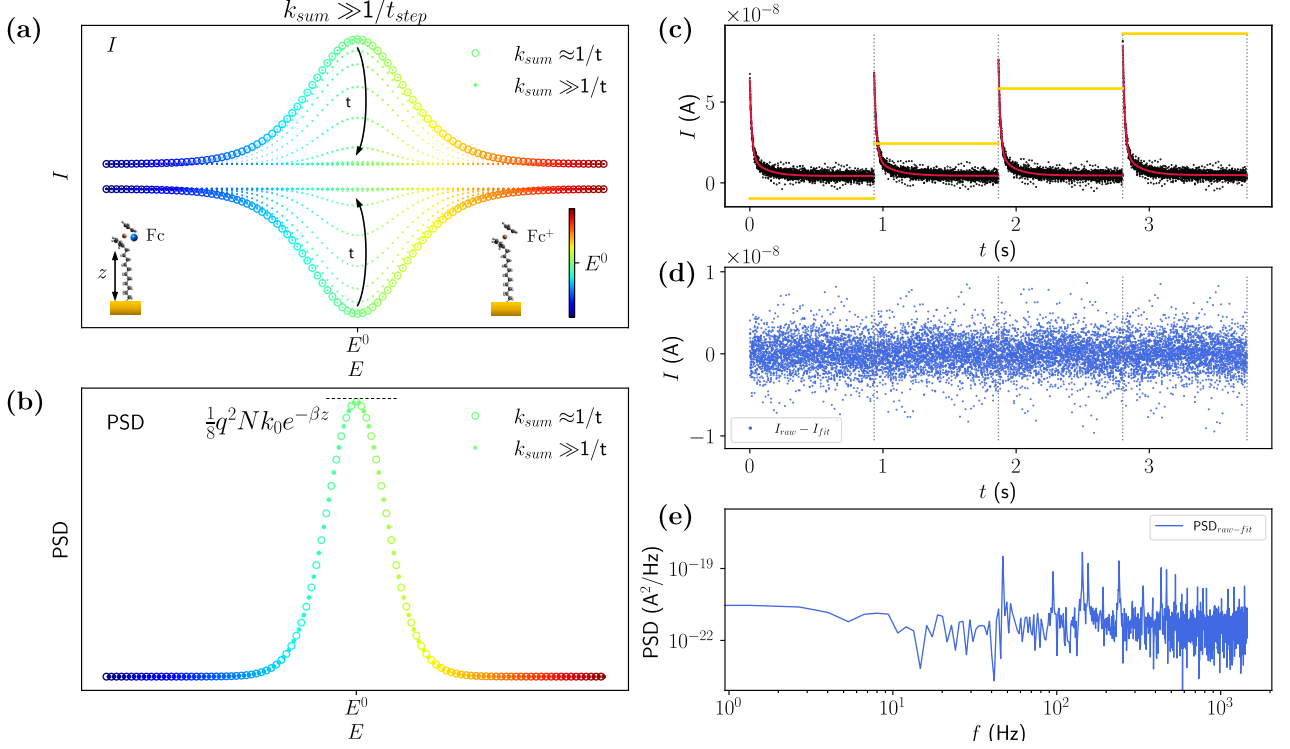


FIG. 1. Illustration of current and noise versus time and voltage, considering a slow scan rate compared to the electron transfer rates ($k_{sum} \gg 1/t_{step}$). (a) I vs E , with the evolution of I as the time after voltage step is increased. (b) Voltnoisograms (PSD vs E) taken at low frequency (Eq. 8) corresponding to the same conditions as in (a). (c) Sampled staircase voltammetry example, with the raw current data (black dots), a double exponential decay fit of the current (red) and the voltage steps (yellow). In this example, each voltage step is of 2.25 mV, starting at 195 mV. (d) Raw currents subtracted with exponential fits (blue). (e) PSD spectrum of one current timetrace in (d).

$$k_{ox,red}^{MH} = \frac{\rho H^2}{\hbar} \sqrt{\frac{\pi}{k_B T \lambda}} \int_{-\infty}^{+\infty} \frac{1}{1 + e^{\frac{x}{k_B T}}} e^{-\frac{(x-\lambda \pm \eta)^2}{4\lambda k_B T}} dx \quad (1)$$

with k_{ox} the oxidation rate, k_{red} the reduction rate, ρ the density of state in the metallic electrode, H^2 the electronic coupling, \hbar the reduced Planck constant, λ the reorganization energy (Frank Condon effect due to water molecules reorganizing after charging the redox molecule), T the temperature, k_B the Boltzmann constant and $\eta = q(E - E^0)$ with E the potential at the electrode, E^0 the standard potential of the molecule and q the elementary charge. Eq.1 is analogue to the Landauer formalism in solid-state physics [8]. The specificity of the redox molecules is their energy level broadening due to the large reorganization energy. Eq.1 can be simplified to Eq. 2 3 (Buttler-Volmer model) when $|\eta| \ll \lambda$ which is often the case. It will be used here initially for its simplicity.

$$k_{ox}^{BV} = k_0 e^{-\beta z} e^{\alpha \frac{\eta}{k_B T}} \quad (2)$$

$$k_{red}^{BV} = k_0 e^{-\beta z} e^{-(1-\alpha) \frac{\eta}{k_B T}} \quad (3)$$

with β the tunneling decay coefficient (1 \AA^{-1}), α the charge transfer coefficient and k_0 the standard electron transfer rate at a distance $z = 0$ (in s^{-1}). The exponential decay part is formally contained in the electronic coupling term H^2 in Eq. 1 but is usually extracted for convenience to be included in the Butler-Volmer model [28].

Sampled current staircase voltammetry (SCV) is the electrochemical technique used to interrogate the surface-attached redox species [29], analogue to the charge pumping technique in semiconductors [30]. The electrode potential is raised in small steps of height E_{step} , and the current is recorded as a function of time, up to a time t_{step} , corresponding to the steps duration (Figure 1 (c)).

The current I , in the case of slow scan rate and long sampling time (i.e. $k_{sum} = k_{ox}^{BV} + k_{red}^{BV} \gg 1/t$), I can be expressed as (details in SM):

$$I = \frac{Nq\nu}{4k_B T} \frac{1}{\cosh^2\left(\frac{\eta}{2k_B T}\right)} \quad (4)$$

with N the total number of molecules and $\nu = E_{step}/t_{step}$ the voltage scan rate. Note that such current represents the transition of the charges at a certain scan rate, and not an equilibrium value of the current at a given potential. Figure 1 (a) shows I versus applied voltage E at a given scan rate and at different times t after the voltage step, exhibiting a quick decrease of amplitude.

One way to consider the noise of the current versus time (Figure 1 (b)) is to look at its power spectrum density (PSD, noted S in equations). The PSD (Figure 1 (b) and (e)) can be seen as a description of how the variance of the measured signal is spread in the frequency domain. The system under study has two-states related to the oxidized/reduced states of the molecules, here attached to a single electrode. Each molecule is expected to lead to the so-called Random Telegraph Signal (RTS) which is a shot noise due to individual transfer of electrons in and out of the single-electron boxes. To avoid confusion, in such a single-electrode system, the shot noise is not expected to be compared to $2qI$ because at equilibrium, where both oxidation and reduction reactions compensate each other, $I = 0$ while $S > 0$ (discussion in SM) [31]. In general, RTS is typically associated with $1/f$ noise due to the wide range of energy levels and electron transfer rates [32, 33]. However, an ensemble of reversible redox couples, like those found in a redox SAM in liquid, can be thought of as an ensemble of quantum dots with very similar energy levels because the molecules that make up the SAM have strictly identical atomic structures and may differ only in their orientation relative to the surface [5]. Assuming first that all N molecules have identical energy levels E^0 and charge transfer rates k_{ox}/k_{red} for oxidation/reduction, respectively, the PSD can be expressed as [32]:

$$S(f, \eta, N) = 4N\Delta I^2 \frac{k_{ox}k_{red}}{k_{ox} + k_{red}} \frac{1}{(k_{ox} + k_{red})^2 + (2\pi f)^2} \quad (5)$$

with f the frequency and ΔI the current corresponding to the oxidation (or reduction) of one molecule. If we consider ΔI as the transfer of one electron of charge q per the average time taken for transferring one electron (i.e., $\Delta I = \frac{q}{\frac{1}{k_{ox}} + \frac{1}{k_{red}}}$), S can be rewritten as:

$$S(f, \eta, N) = 4Nq^2 \frac{(k_{ox}k_{red})^3}{(k_{ox} + k_{red})^3} \frac{1}{(k_{ox} + k_{red})^2 + (2\pi f)^2} \quad (6)$$

which becomes at low frequency (assuming $\alpha = 0.5$):

$$\lim_{f \rightarrow 0} S(\eta, N) = 4Nq^2 \frac{(k_{ox}k_{red})^3}{(k_{ox} + k_{red})^5} \quad (7)$$

$$= \frac{1}{8} Nq^2 \frac{k_0 e^{-\beta z}}{\cosh^5\left(\frac{\eta}{2k_b T}\right)} \quad (8)$$

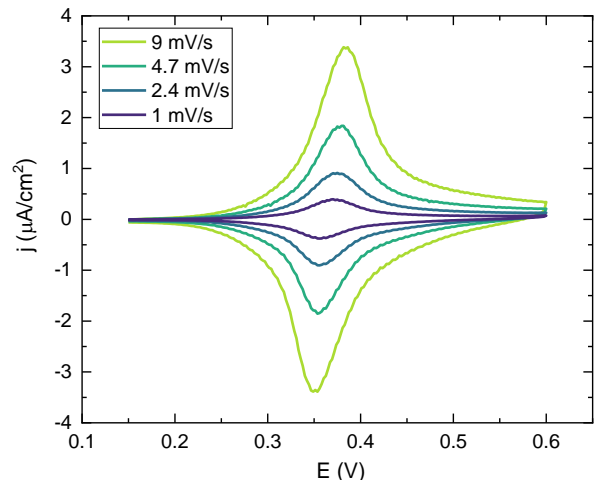


FIG. 2. Example of current CVs obtained at different ν (electrode area $\approx 45 \text{ mm}^2$, E vs Ag/AgCl (3 M NaCl), electrolyte: $[\text{NaClO}_4]=0.5 \text{ M}$).

This equation expresses the dependence of the low frequency electrochemical shot noise of the redox SAM versus the electrode potential. The corresponding curve is plotted in Figure 1 (b). Similarly to current SCV signals, it presents a peak at E^0 , but narrower than that of the SCV peak, with a full width at half-maximum (FWHM):

$$E_{FWHM}^S = 4 \text{acosh}(\sqrt[5]{2}) \frac{k_B T}{q} \approx 56 \text{ mV} \quad (9)$$

Note that unlike the current, S does not depend on ν as the PSD is considered for a system at equilibrium. S is also independent of the potential scan direction. Interestingly, the limiting cases of $\eta \rightarrow 0$ and $f \rightarrow 0$ give access to the electron transfer rate k_0 and the total number of molecules N .

$$\lim_{\eta \rightarrow 0} S(f, N) = \frac{1}{2} Nq^2 k_0 e^{-\beta z} \frac{1}{4 + \left(\frac{2\pi f}{k_0 e^{-\beta z}}\right)^2} \quad (10)$$

with the corner frequency $f_c = \frac{1}{2\pi} k_0 e^{-\beta z}$:

$$\lim_{\eta \rightarrow 0, f \rightarrow 0} S(N) = \frac{1}{8} Nq^2 k_0 e^{-\beta z} \quad (11)$$

The main result of the present work is Eq. 11, linking directly and simply k_0 and N to the noise measured at low frequency for $E = E^0$. Provided the corner frequency of the PSD f_c can be measured (Figure S1 (b)), the individual values of k_0 and N are obtained from Eq. 10 and Eq. 11. Alternatively, if N is known independently, k_0 can be straightforwardly derived from S at $E = E^0$ (Eq. 11).

To demonstrate the validity of the previous analysis, an experiment is set using ferrocene undecanethiol $\text{Fc}(\text{CH}_2)_{11}\text{SH}$ self-assembled on a gold microelectrode. A two-electrode electrochemical cell setup is used in a Faraday cage, using a $[\text{NaClO}_4]=0.5$ M aqueous electrolyte and a Ag/AgCl electrode (3 M NaCl) acting as both reference and counter electrode. Details about the sample preparation and the measurement setup can be found in Supplementary Materials (Figure S2 and S3). The system is interrogated using staircase voltammetry (Figure 1 (c)), which is equivalent to linear cyclic voltammetry (CV) at slow scan rates [34]. Our motivation is to offer a comparison of the well-known technique of cyclic voltammetry with the results obtained looking at the shot noise of the system.

The Figure 2 shows an example of current CVs at different (low) scan rates ν . The signal is centered around a potential value of $E^0 = 0.35 \pm 0.02$ V vs Ag/AgCl , which corresponds to the expected standard potential for such surface-attached Fc molecules [35–37]. The density is estimated here at 4.2×10^{-10} mol/cm², close to the values reported in the literature for packed SAMs ($4.4 \sim 4.9 \times 10^{-10}$ mol/cm²) [1, 38]. The peak current of the CV exhibit the usual behavior for a surface-confined reversible couple, with a linear dependency of the current versus ν (example data Figure S11).

PSD signals were measured at several scan rates (see details in SM), their magnitude at 20 Hz versus E (called “voltnoisogram” for concision) shown in Figure 3 (a), (full set Figure S12). Similar data without the Fc molecules can be found in Figure S10. The PSD voltnoisograms behave as expected with a peak-shaped curve centered around $E^0 \approx 0.35$ V, close to the standard potential of Fc. As predicted from Eq. 8, the peak value of the PSD voltnoisograms (Figure 3 (b)) remains quasi-constant for $\nu < 3$ mV/s (see details in SM Figure 3).

Figure 4 (a) shows a cyclic voltammetry (CV) scan at $\nu = 0.014$ mV/s where no faradaic current signal can be identified. Figure 4 (b) shows power spectral density (PSD) values at $E < E^0$, $E \approx E^0$ and $E > E^0$ on the forward scan. Figure 4 (c) shows the variation of PSD at 10 Hz as a function of the voltage, showing a clear peak. These results demonstrate the ability to detect an electrochemical reaction at an electrode through shot noise measurements, even when the average current signal from the CV does not show any reaction. The number of molecules $N = 7.5 \times 10^{10}$ is calculated from the CV data at higher scan rates (Figure S11), and using this value and Eq. 11, the peak amplitude of PSD data shown in Figure 3 yields $k_0 = 6.3 \times 10^7$ s⁻¹ ($z = 1$ nm) is in good agreement with literature values for this molecule[15, 20].

The FWHM of the PSD peaks on Figure 4 is ≈ 90 mV, broader than the 56 mV predicted by Eq. 9. Taking $\eta = 0$ in the Eq. 1 gives an expression for k_0 , notably showing dependencies with H and λ [28]. Previous work

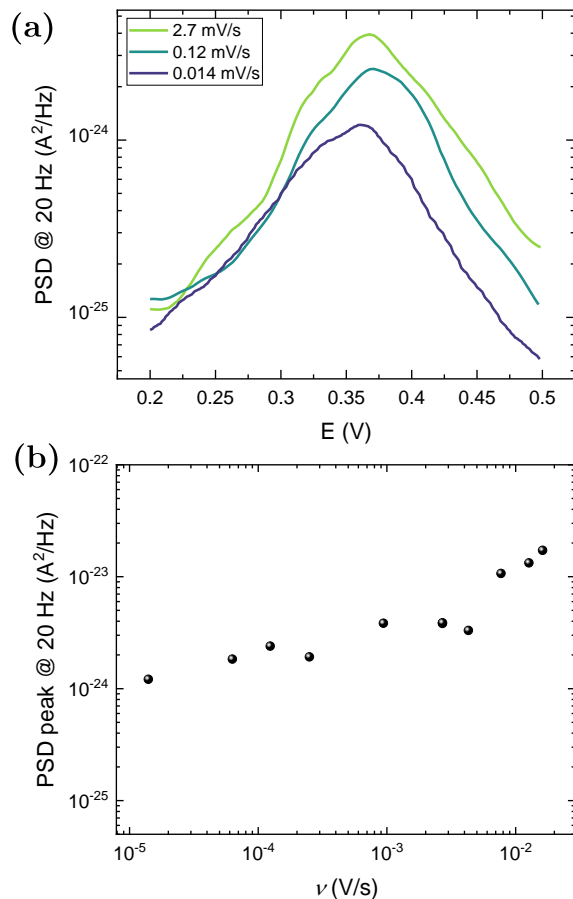


FIG. 3. (a) PSD of the current versus E obtained at different ν , at $f \approx 20$ Hz. (b) PSD at $f \approx 20$ Hz and $E = 0.35$ V versus ν .

[15] showed that variation of λ within physically reasonable limits do not significantly impact the electron transfer rates. However, the electronic coupling term H typically varies following lognormal distributions [5] and can impact significantly the resulting value of k_0 with variations of just a few percent of its average value (see Figure S13 & S14). If a lognormal distribution of the fluctuation of H (and thus, of k_0 as well) is assumed, a standard deviation of $\sigma \approx 4\%$, comparable to what was reported in ref [5] ($\approx 2\%$), can explain the broadening observed in PSD (Figure 4 (c) dashed line).

There is a significant difference between molecular monolayers in liquid and solid-state devices in terms of electrostatic forces. In the first case, the electrostatic interactions between neighboring molecules are greatly reduced thanks to the high permittivity of water. Previous research on $\pi - \pi$ coulomb repulsion φ (Eq. 12) within similar Fc SAMs showed negligible impact on current CV [5, 39].

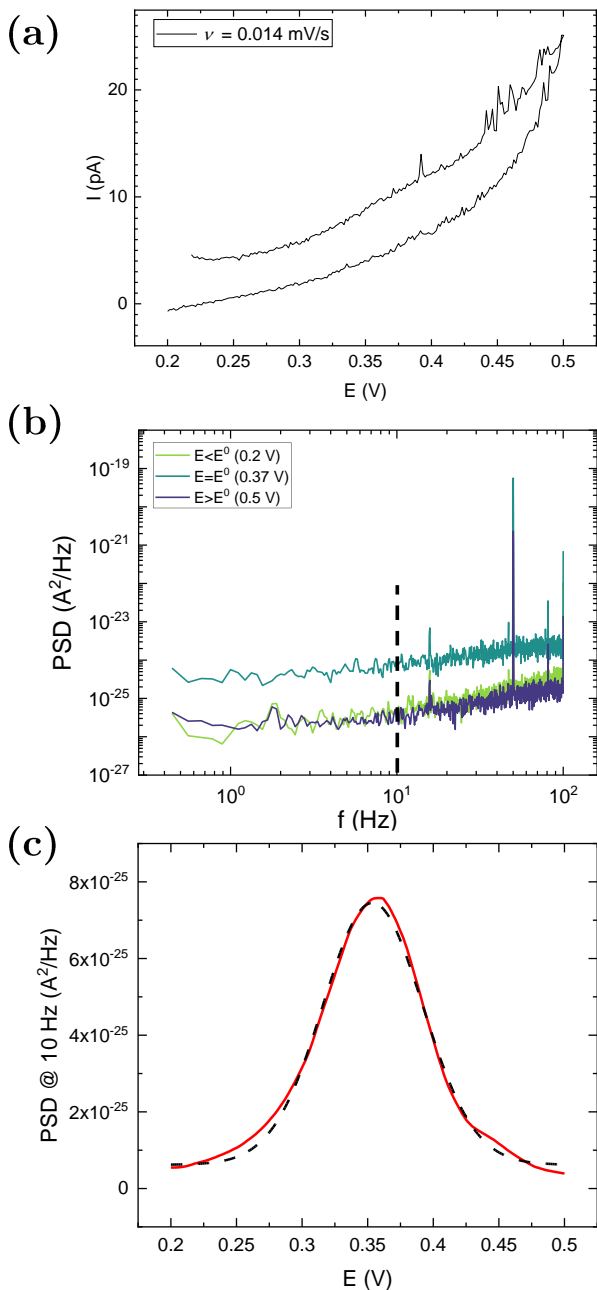


FIG. 4. (a) CV of a FcC₁₁SH SAM on gold. (b) PSD measured at 0.014 mV/s at $E < E^0$, $E \approx E^0$ and $E > E^0$. (c) PSD versus potential at 10 Hz. The dashed line is fitted using Eq. 7 considering a lognormal distribution of H with $\sigma = 3.97\%$ of the mean value of H .

$$\varphi = q \frac{1 - \left(1 + \left(\frac{r_a}{d}\right)^2\right)^{-0.5}}{4\pi\epsilon_0\epsilon_r d} \quad (12)$$

with d the intermolecular distance, r_a the distance to counter ions, ϵ_0 the permittivity of the vacuum and $\epsilon_r = \epsilon_{H_2O}|\epsilon_{SiO_2}$ the permittivity of the medium under

consideration. Taking the same formalism and distribution of d as in [5] for φ but changing $\epsilon_{H_2O} = 79$ to $\epsilon_{SiO_2} = 3.9$ results in variations of E_{FWHM}^S from 1% to 45% respectively (see Figure S15 & S16). As a result the screening of electrostatic interaction by water avoids a dispersion of the energy levels, such as the one observed in nanotransistors [33], and thus, avoids the domination of a $1/f$ noise resulting from the sum of multiple Lorentzian spectra with different amplitude/corner frequencies.

In conclusion, we demonstrated the measurement of the shot noise generated by an ensemble of surface-attached Fc redox molecules, which can be seen as identical single-electron boxes, in liquid and in ambient conditions. A formalism is proposed to understand it and exhibit dependencies between such noise and electronic coupling. This constitutes a further step toward nanoelectrochemistry and single molecule measurements, which could be practically achieved using our technique combined with a transducer such as a nanotransistor and be extended to other systems such as quantum dots monolayer [40].

Our technique allows for the measurement of electron transfer rates at low frequencies without the need for highly time-resolved instrumentation. Although we compared our technique with traditional voltammetry techniques, exhibiting a clear signal in PSD when I tended to zero, the very concept of “potential scan” is actually not required to perform noise measurements. As few as two points at potentials far from E^0 and one at E^0 can suffice to resolve the eventual background noise of the experiment and the noise due to the attached molecule, yielding k_0 and N provided the knowledge of β and z . Concurrently, since the measurements is carried out at equilibrium, capacitive contributions are altogether avoided, improving the signal and simplifying drastically the interpretation of the data. This opens perspectives in the field of biosensors [11], where the limit of detection of existing techniques could be further extended by shot noise analysis, and in high-frequency molecular diodes, where the electron transfer rate can be estimated through the low-frequency noise.

ACKNOWLEDGMENTS

This work has been supported by the EU-ATTRACT project (Unicorn-Dx), the French “Agence Nationale de la Recherche”(ANR) through the “SIBI” project (ANR-19-CE42-0011-01) and the JSPS Core-to-Core Program (JPJSCCA20190006).

S.G designed the acquisition system, conducted the experiments and data analysis and developed the theory, S.L. fabricated the devices, L.J. designed the acquisition system, SH. K. and A.C. contributed to the scientific in-

teractions on electrochemistry, C.D. and N.C. conceived and supervised the whole project. All authors actively contributed to the discussions and the writing of the paper.

-
- [1] J. Trasobares, D. Vuillaume, D. Théron, and N. Clément, *Nature Communications* **7**, 12850 (2016).
- [2] C. Reynaud, D. Duché, J.-J. Simon, E. Sanchez-Adame, O. Margeat, J. Ackermann, V. Jangid, C. Lebouin, D. Brunel, F. Dumur, D. Gimes, G. Berginc, C. Nijhuis, and L. Escoubas, *Progress in Quantum Electronics* **72**, 100265 (2020).
- [3] N. Clement and A. Fujiwara, *Nature Nanotechnology* **12**, 725 (2017).
- [4] X. Chen, M. Roemer, L. Yuan, W. Du, D. Thompson, E. del Barco, and C. A. Nijhuis, *Nature Nanotechnology* **12**, 797 (2017), number: 8 ZSCC: NoCitationData[s0].
- [5] J. Trasobares, J. Rech, T. Jonckheere, T. Martin, O. Aleveque, E. Levillain, V. Diez-Cabanes, Y. Olivier, J. Cornil, J. P. Nys, R. Sivakumarasamy, K. Smaali, P. Leclere, A. Fujiwara, D. Théron, D. Vuillaume, and N. Clément, *Nano Letters* **17**, 3215 (2017).
- [6] Y. Li, D. Wang, W. Peng, L. Jiang, X. Yu, D. Thompson, and C. A. Nijhuis, *Nano Today* **44**, 101497 (2022).
- [7] P. Gehring, J. M. Thijssen, and H. S. J. van der Zant, *Nature Reviews Physics* **1**, 381 (2019).
- [8] K. H. Bevan, M. S. Hossain, A. Iqbal, and Z. Wang, *The Journal of Physical Chemistry C* **120**, 179 (2016).
- [9] A. Nitzan and M. A. Ratner, *Science* **300**, 1384 (2003).
- [10] R. A. Marcus, *The Journal of Chemical Physics* **24**, 966 (1956).
- [11] S. Li, Y. Coffinier, C. Lagadec, F. Cleri, K. Nishiguchi, A. Fujiwara, T. Fujii, S.-H. Kim, and N. Clément, *Biosensors and Bioelectronics* **216**, 114643 (2022).
- [12] F.-R. F. Fan, J. Kwak, and A. J. Bard, *Journal of the American Chemical Society* , 7 (1996).
- [13] S. Grall, I. Alić, E. Pavoni, M. Awadein, T. Fujii, S. Müllegger, M. Farina, N. Clément, and G. Gramse, *Small* **17**, 2101253 (2021).
- [14] S. Huang, M. Romero-Ruiz, O. K. Castell, H. Bayley, and M. I. Wallace, *Nature Nanotechnology* **10**, 986 (2015).
- [15] C. E. D. Chidsey, *Science* **251**, 919 (1991).
- [16] C. Demaille, N. Clément, A. Chovin, S. H. Kim, and Z. Zheng, *ChemXiv* 10.26434/chemrxiv-2022-212hs (2022), preprint.
- [17] Y. Blanter and M. Büttiker, *Physics Reports* **336**, 1 (2000).
- [18] D. Djukic and J. M. van Ruitenbeek, *Nano Letters* **6**, 789 (2006).
- [19] O. S. Lumbroso, L. Simine, A. Nitzan, D. Segal, and O. Tal, *Nature* **562**, 240 (2018).
- [20] M. A. G. Zevenbergen, B. L. Wolfrum, E. D. Goluch, P. S. Singh, and S. G. Lemay, *Journal of the American Chemical Society* **131**, 11471 (2009).
- [21] K. Mathwig, D. Mampallil, S. Kang, and S. G. Lemay, *Physical Review Letters* **109**, 118302 (2012).
- [22] E. Kätelhön, K. J. Krause, P. S. Singh, S. G. Lemay, and B. Wolfrum, *Journal of the American Chemical Society* **135**, 8874 (2013).
- [23] P. S. Singh and S. G. Lemay, *Analytical Chemistry* **88**, 5017 (2016).
- [24] P. Karnatak, T. Paul, S. Islam, and A. Ghosh, *Advances in Physics: X* **2**, 428 (2017).
- [25] E. Paladino, Y. Galperin, G. Falci, and B. Altshuler, *Reviews of Modern Physics* **86**, 361 (2014).
- [26] N. Clément, S. Pleutin, O. Seitz, S. Lenfant, and D. Vuillaume, *Physical Review B* **76**, 205407 (2007).
- [27] A. Fragasso, S. Schmid, and C. Dekker, *ACS Nano* **14**, 1338 (2020).
- [28] J. F. Smalley, S. W. Feldberg, C. E. D. Chidsey, M. R. Linfood, M. D. Newton, and Y.-P. Liu, *The Journal of Physical Chemistry* **99**, 13141 (1995).
- [29] H. A. Heering, M. S. Mondal, and F. A. Armstrong, *Analytical Chemistry* **71**, 174 (1999).
- [30] A. Fujiwara, K. Nishiguchi, and Y. Ono, *Applied Physics Letters* **92**, 042102 (2008).
- [31] R. Sarpeshkar, T. Delbruck, and C. Mead, *IEEE Circuits and Devices Magazine* **9**, 23 (1993), number: 6.
- [32] S. Machlup, *Journal of Applied Physics* **25**, 341 (1954).
- [33] N. Clément, K. Nishiguchi, A. Fujiwara, and D. Vuillaume, *Nature Communications* **1**, 92 (2010).
- [34] J. H. Christie and P. J. Lingane, *Journal of Electroanalytical Chemistry* (1959) **10**, 176 (1965).
- [35] H. Tian, Y. Dai, H. Shao, and H.-Z. Yu, *The Journal of Physical Chemistry C* **117**, 1006 (2013).
- [36] N. Nerngchamnong, D. Thompson, L. Cao, L. Yuan, L. Jiang, M. Roemer, and C. A. Nijhuis, *The Journal of Physical Chemistry C* **119**, 21978 (2015).
- [37] N. K. Gupta, E. A. Wilkinson, S. K. Karuppanan, L. Bailey, A. Vilan, Z. Zhang, D.-C. Qi, A. Tadich, E. M. Tuite, A. R. Pike, J. H. R. Tucker, and C. A. Nijhuis, *Journal of the American Chemical Society* **143**, 20309 (2021).
- [38] C. A. Nijhuis, W. F. Reus, and G. M. Whitesides, *Journal of the American Chemical Society* **131**, 17814 (2009).
- [39] M. G. Reuter, M. C. Hersam, T. Seideman, and M. A. Ratner, *Nano Letters* **12**, 2243 (2012).
- [40] J. M. Fruhman, H. P. Astier, B. Ehrler, M. L. Böhm, L. F. L. Eyre, P. R. Kidambi, U. Sassi, D. De Fazio, J. P. Griffiths, A. J. Robson, B. J. Robinson, S. Hofmann, A. C. Ferrari, and C. J. B. Ford, *Nature Communications* **12**, 4307 (2021).

Electrochemical Shot Noise of a Redox Monolayer

Supplementary Material

Simon Grall, Shuo Li, Laurent Jalabert, Soo-Hyeon Kim and Nicolas Clément

IIS, LIMMS/CNRS-IIS IRL2820, The Univ. of Tokyo; 4-6-1 Komaba,

Meguro-ku Tokyo, 153-8505, Japan

Arnaud Chovin, Christophe Demaille

Université Paris Cité, CNRS, Laboratoire

d'Electrochimie Moléculaire, F-75013 Paris, France

(Dated: March 6, 2023)

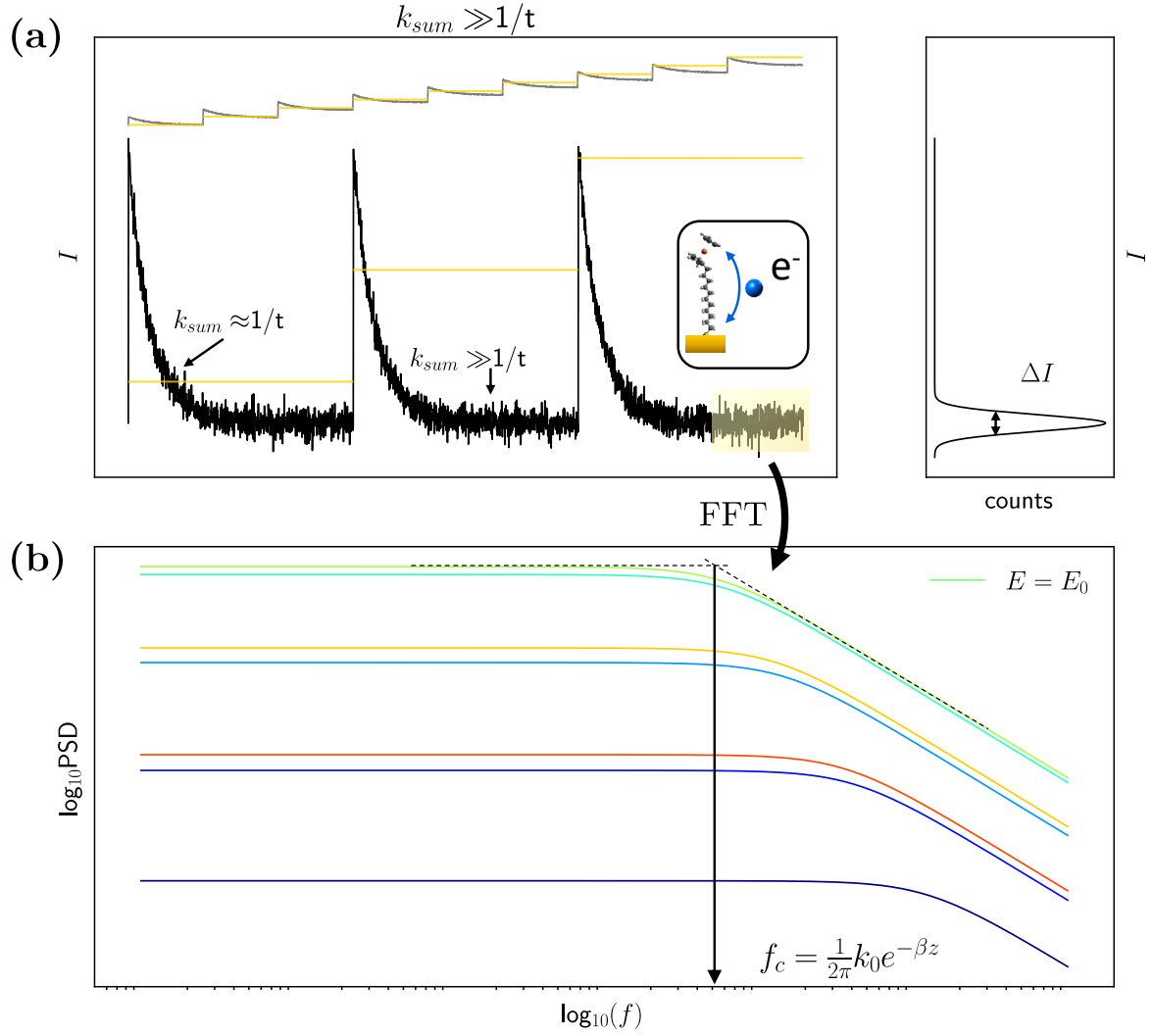


FIG. S1. (a) Computer-generated time traces of the current for illustrative purposes, with long waiting time such as I reaches zero at each voltage step (black). Voltage steps E_{step} are represented in yellow. The right panel represents the distribution of the current around its average, with ΔI as described in the main text. (b) Noise versus frequency for different E , with the corner frequency indicated for $E = E^0$. The noise data are obtained at each E_{step} by Fourier transform of the autocorrelation of the current data when the average current reaches zero (yellow window on (a)).

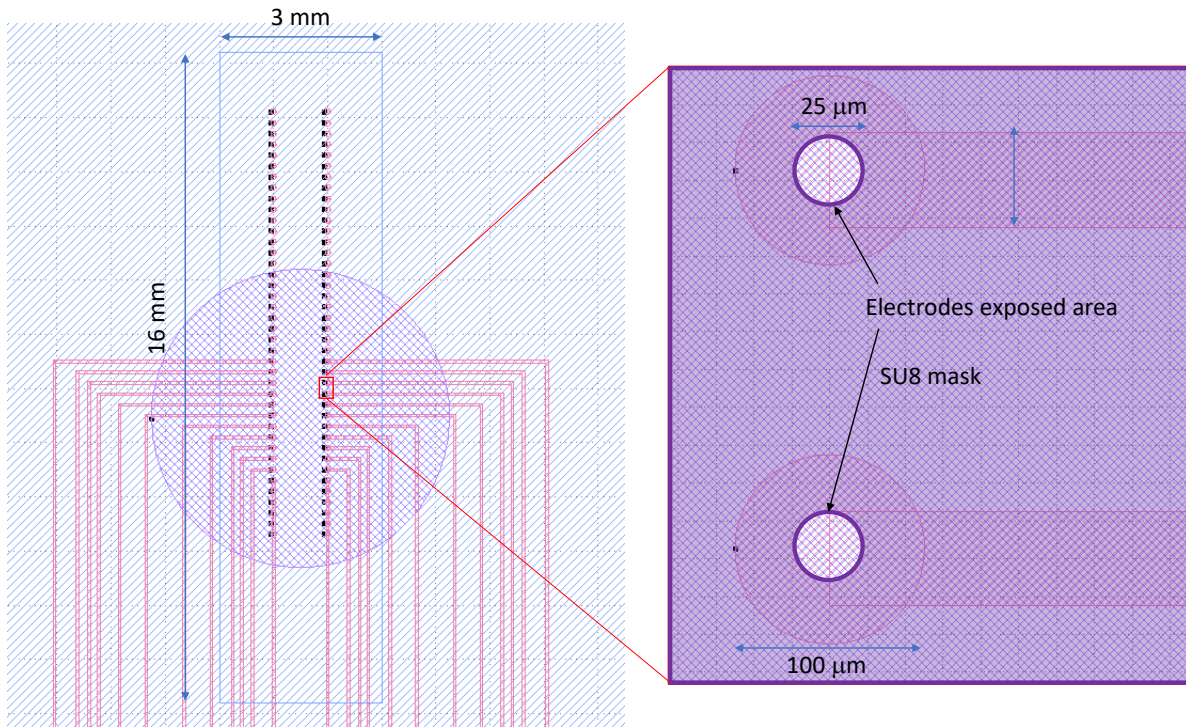


FIG. S2. Layout of the microelectrodes used, with a zoom on the right indicating the exposed area and the SU8 mask.

SAMPLE PREPARATION

The electrode is fabricated by gold sputtering on a silicon wafer. Plain electrodes (From 45 mm² down to 0.78 mm²) and microelectrodes (as described Figure S2) were used. The later was preferred for noise measurements, as in a 2-electrode electrochemical setup, keeping low-current to avoid potential drop is critical. For the microelectrodes configuration, a layer of SU8 (thickness = 25 μm) is spin-coated on all the wafer except the designated gold areas to prevent unwanted reactions with silicon dioxide and limit the parasitic capacitance (Figure S2). The electrode is incubated in a 1 mM ethanol solution of ferrocene undecanethiol for at least one day, with further incubation in a 1 mM undecanethiol solution for 2h. CV curves Figure S11 were used to extract $N = 7.5 \pm 0.05 \times 10^{10}$. The electrochemical experiments are all carried out in 0.1 M NaClO₄ aqueous electrolyte and after N₂ bubbling. The electrochemical cell (SEC-3F, ALS Co., Japan) is made of a small silicon gasket delimiting a channel (3 × 16 × 0.3 mm) over the microelectrodes and connected to the Ag/AgCl electrode. The cell can be sealed with microfluidic switches after filling with the electrolyte.

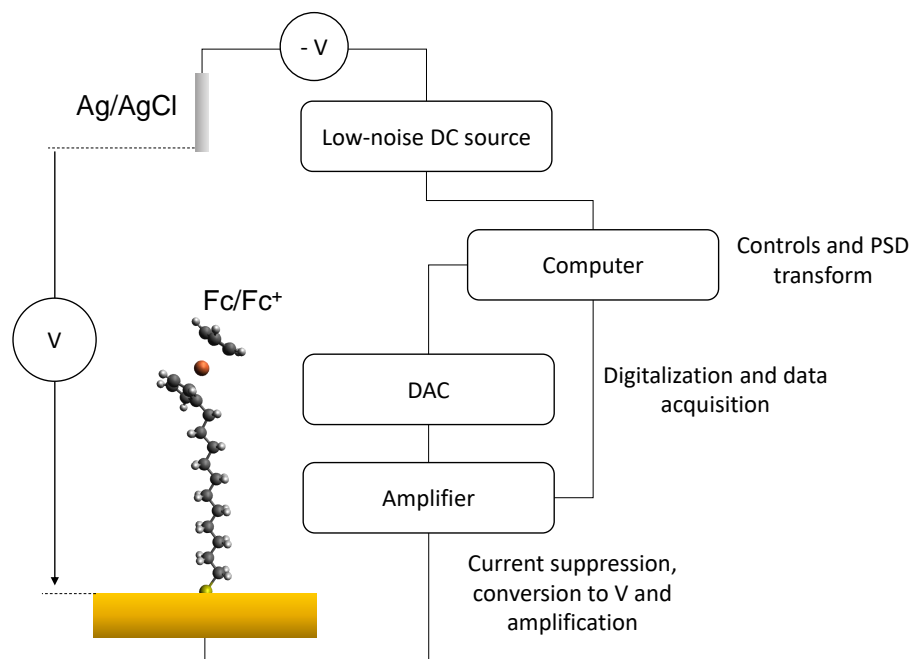


FIG. S3. Schematics of the setup used to scan the voltage over the Fc SAM and recover the current and PSD data.

MEASUREMENT SETUP

The microelectrodes are connected to a current amplifier (CA5351, NF Corporation, Japan), itself connected to a digital-to-analog converter (USB-4431, National Instrument) (Figure S3). The voltage is applied using a Ag/AgCl (3 M NaCl) reference electrode. Though only two electrodes are used, the very low currents expected make the voltage drop across the electrochemical cell negligible. As a control, we verified that experiments carried out in a three-electrode configuration (using a platinum wire counter electrode) yielded similar results as those obtained with our two-electrode setup. The whole experiment is controlled using a Labview program. As a precaution, a platinum counter electrode is added to the setup and cyclic voltammograms are measured both with and without the counter electrode, with no significant differences.

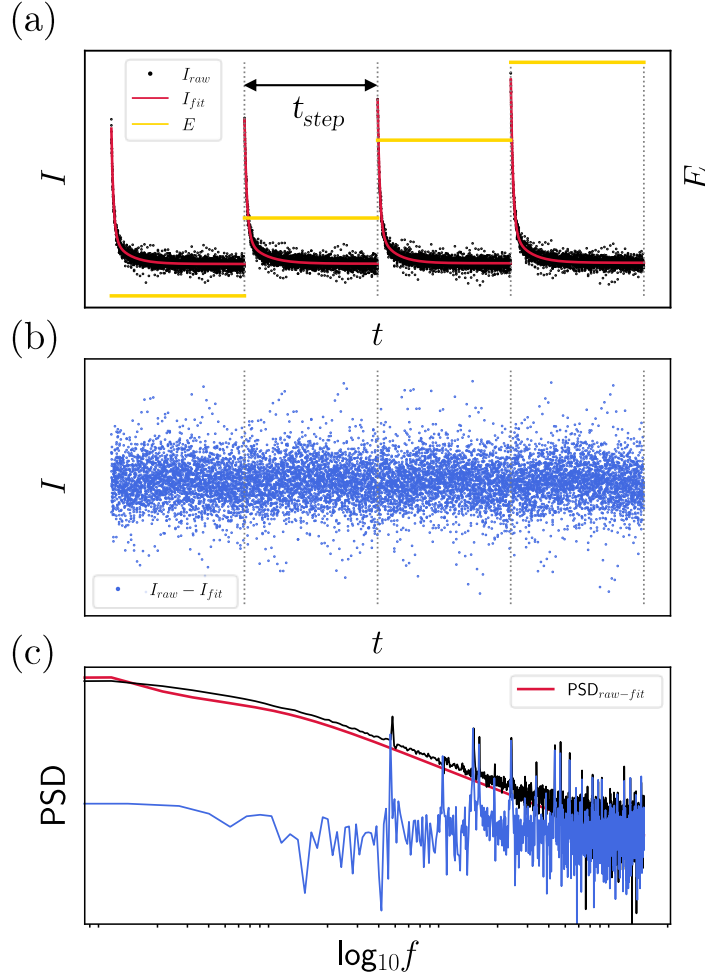


FIG. S4. (a) Staircase voltammetry example, with the raw current data (black dots), a double exponential decay fit of the current (red) and the voltage steps (yellow). (b) Flattened currents (raw current corrected by the subtraction of exponential fits). (c) PSD spectrum of one current time trace obtained using the raw current subtracted with the exponential fit (blue). The black line represents the PSD obtained from raw data, and the red one from the exponential fits.

EXPERIMENTAL MEASUREMENTS CONDITIONS

To avoid the contribution of any transient current, two types of measurements are realized. The first one corresponds to staircase sampled current experimental conditions (“SCV conditions”). For each potential step E_{step} the whole timetrace of the current is recorded and fitted with a double exponential decay (Figure 1 (c), details in Figure S5 and S6):

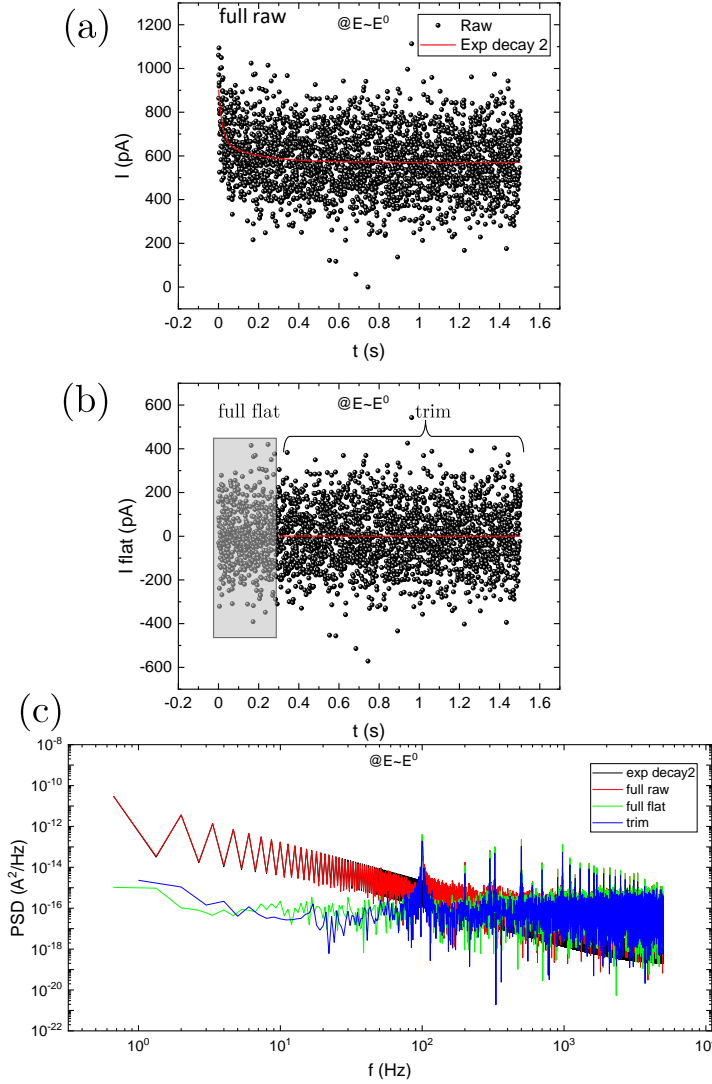


FIG. S5. (a) Raw current data trace, a double exponential decay fit of the current is shown (red). (b) Flattened current (raw currents corrected by the subtraction of exponential fits) with only the last 4/5th kept for PSD calculation. (c) PSD spectra obtained from raw data (black), exponential fits (red), flattened current (green) and trimmed flattened current (blue). The later is used throughout this work for processing "CV conditions" data.

$$I = A_c e^{-\frac{t}{\tau_c}} + A_f e^{-\frac{t}{\tau_f}} \quad (\text{S1})$$

with (A_c, τ_c) the amplitude and time constant of the capacitive current, due to the relaxation of the double layer, and (A_f, τ_f) the amplitude and time constant of the faradaic

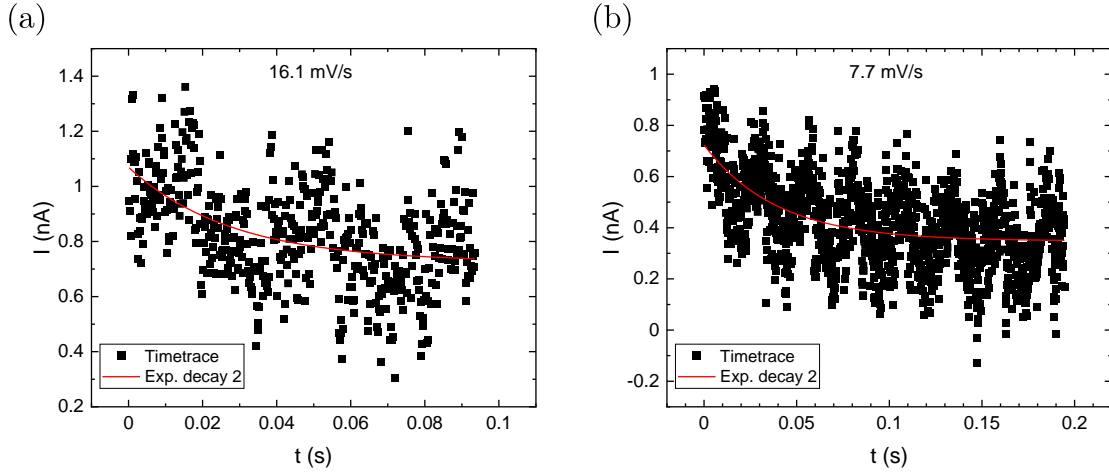


FIG. S6. time traces recorded at $E = E^0$ at (a) 16.1 mV/s and (b) 7.7 mV/s. The fitting lines are obtained using Eq. S1

current, due to the charge transfer between Fc molecules and the electrode. Typical time constants were on the order of 0.1 s and 0.01 s for τ_f and τ_c respectively. The PSD spectra are extracted from “flattened” currents, obtained by subtracting the exponential decay contribution (Figure 1 (d), details in Figure S1 – S6). For $t_{step} > 5 \times \max(\tau_c, \tau_f)$ (here corresponding to $\nu < 10$ mV/s), the transients were well-resolved and the low-frequency noise could be acquired using this method (Figure 1 (e)). For $\nu < 10$ mV/s, the time trace was fitted, straightened and trimmed, keeping only the 4/5th of the time trace to calculate the PSD (Figure S4). The resulting PSD does not vary significantly as shown in Figure 3, which supports $t > 5 \times \tau$ criteria being reasonable.

Noise conditions

The second type of measurement, called here “Noise conditions” consists in using very slow scan rates ($\nu < 0.1$ mV/s) in order to bring the system as close as possible to equilibrium at each electrode potential value (Figure S1). Several time traces are recorded at each voltage step, giving time to the system to reach equilibrium for a given voltage ($k_{sum} \gg 1/t$), meaning that after the initial time trace recorded just after the voltage change, no transient phenomenon occurs. In this case, the mean current tends to zero (Figure 1 (a) and (c)), but

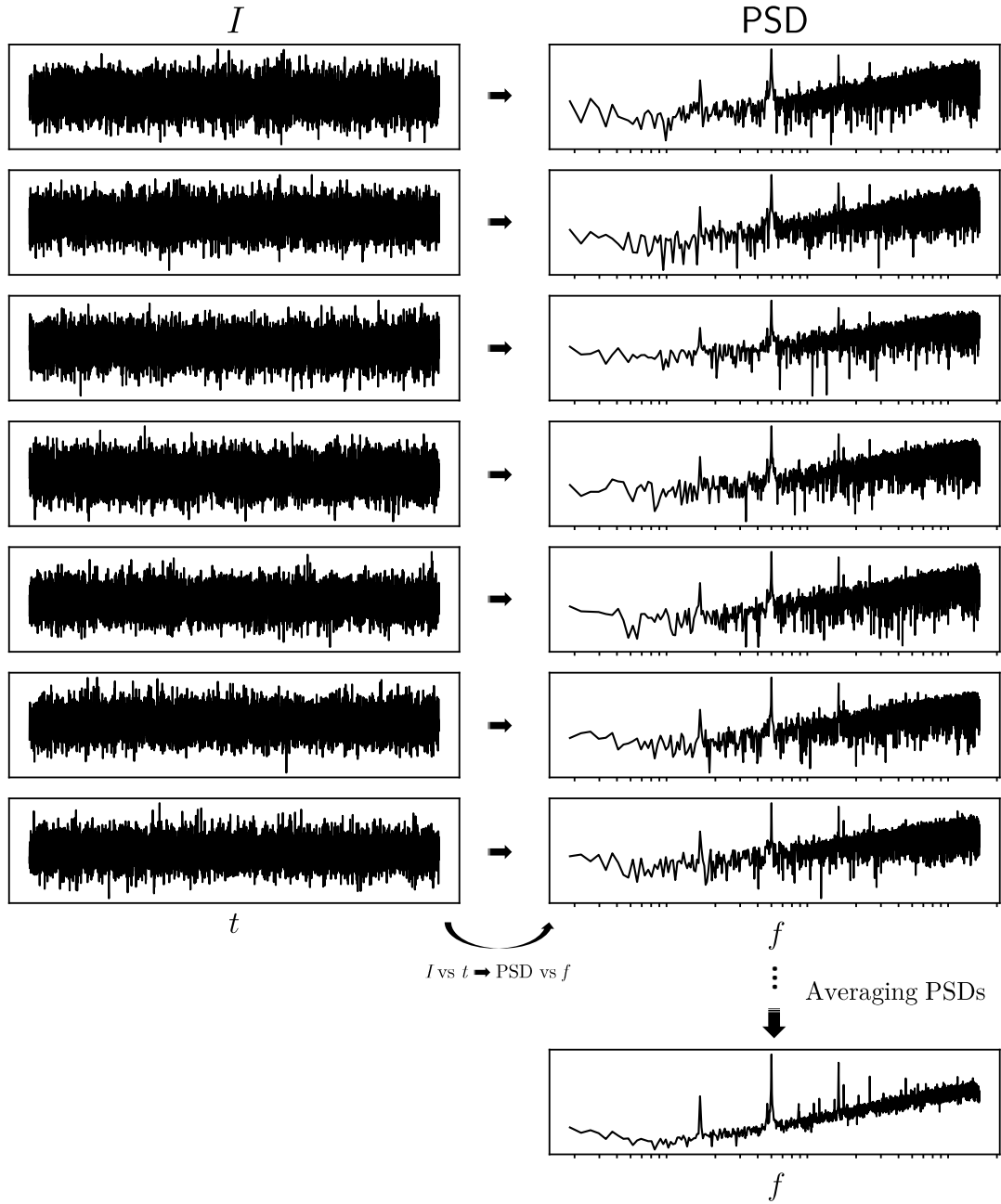


FIG. S7. Illustration for the "Noise conditions" measurements. For each voltage step, the current is measured n times ($n = 7$ in this example, $n > 10$ during experiments) during a time window of t and converted into PSD (plotted versus the frequency f). After n measurements, the PSDs obtained are averaged over n (bottom right graph) and the measurement restarts at the next voltage step.

not the noise (Figure 1 (b) and S1). This allows to average the PSD obtained from each time trace at least 10 times (Figure S7), and this for each voltage step with no transient contribution to the PSD. The other consequence is that the effective voltage scan rates are very low, on the order of 0.1 mV/s and below. The measure of the noise out of equilibrium (if it can still be called "noise" in such case) is possible but is beyond the scope of the present article.

In Figure 3, PSD measurements were carried out from $\nu = 1$ mV/s up to 16.1 mV/s only, due to transients interfering at higher scan rates. Lower scan rates were measured using the Noise conditions.

CYCLIC VOLTAMMETRY CURRENTS

The probability $P_{ox}(E)$ for a molecule to be oxidized at a given voltage E after time t can be written as :

$$P_{ox} = \frac{k_{ox}^{BV}}{k_{sum}} (1 - e^{-(k_{sum} t_{step})}) \quad (\text{S2})$$

with $k_{sum} = k_{ox}^{BV} + k_{red}^{BV}$, $\nu = E_{step}/t_{step}$ the voltage scan rate. In the case where the electron transfer is fast compared to the time spent at each step ($k_{sum} \gg 1/t_{step}$), P_{ox} simplifies to:

$$P_{ox} = \frac{k_{ox}^{BV}}{k_{sum}} = \frac{1}{1 + e^{-\frac{\eta}{k_B T}}} \quad (\text{S3})$$

The proportion of attached molecules being effectively oxidized at a given time is approaching P_{ox} following an exponential decay as all molecules end up in the equilibrium state. Defining the current I as the number of transferred charges per unit of time, the current is:

$$I = Nq \frac{dP_{ox}}{dt_{step}} = Nq\nu \frac{dP_{ox}}{dE_{step}} \quad (\text{S4})$$

with N the total number of molecules. For the rest of the study, unless mentioned otherwise, we consider the case of relatively slow scan rates, where electron transfer rates are large compared to the inverse of the time spent at each voltage step ($k_{sum} \gg 1/t_{step}$). t is defined here as the sampling time, with $0 \leq t \leq t_{step}$. In this case, for long sampling times (i.e. $k_{sum} \gg 1/t$), $P_{ox} = k_{ox}/k_{sum}$ and I simplifies to:

$$I = \frac{Nq\nu}{4k_B T} \frac{1}{\cosh^2\left(\frac{\eta}{2k_B T}\right)} \quad (\text{S5})$$

with a full width at half maximum (FWHM):

$$E_{FWHM}^I = 4 \operatorname{acosh}(\sqrt{2}) \frac{k_B T}{q} \approx 90.6 \text{ mV} \quad (\text{S6})$$

where acosh is the inverse of the hyperbolic cosine (considering $T = 298 \text{ K}$ for the numerical value) [1, 2].

DIELECTRIC LOSSES

The PSD spectra exhibit a $\tan(\delta)$ dielectric loss contribution:

$$S_D(f) = 8k_B T \pi C \tan(\delta) f \quad (\text{S7})$$

with C the capacitance and $\tan(\delta)$ the dielectric loss tangent [3, 4]. Negligible at low-frequency, the dielectric noise allows access to the low-frequency shot noise, but unfortunately not to f_c . The origin of the dielectric losses noise can be attributed to the SAM's capacitance. Considering the area of the exposed electrode ($A = 7.84 \times 10^{-9} \text{m}^2$) and the capacitance of the SAM ($C = 1.5 \times 10^{-8} \text{F}$), PSD acquired far from V_0 can be fit with Eq. S7 (Figure S8) with dielectric losses around 1, slightly higher than measured in dry [5] and on the order of common polymer [6]. However, this assumes a constant $\tan(\delta)$ with frequency, which is not necessarily the case if for example, water molecules penetrate the SAM. The curve obtained at E^0 Figure S8 seems to suggest a non-constant loss with frequency. Though beyond the scope of the current work, further investigations could allow to use such noise measurements as a probing method for the effective capacitance of the SAM[7]. The very small scaling of the PSD peak value with ν confirms that the measurement of the noise is well-suited for the study of systems with small numbers of charge carriers, high electron transfer rates and at very slow scan rates, where the parasitic capacitive currents can be suppressed.

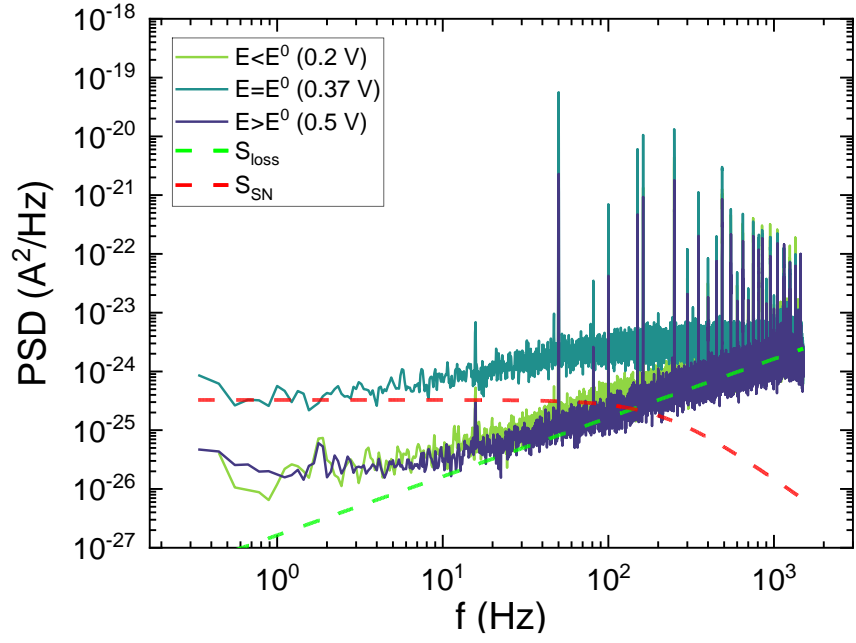


FIG. S8. Full PSD spectrum with partial fits (dashed lines) of dielectric noise losses (red) at $E \ll E^0$ and electrochemical shot noise (green) at $E = E^0$.

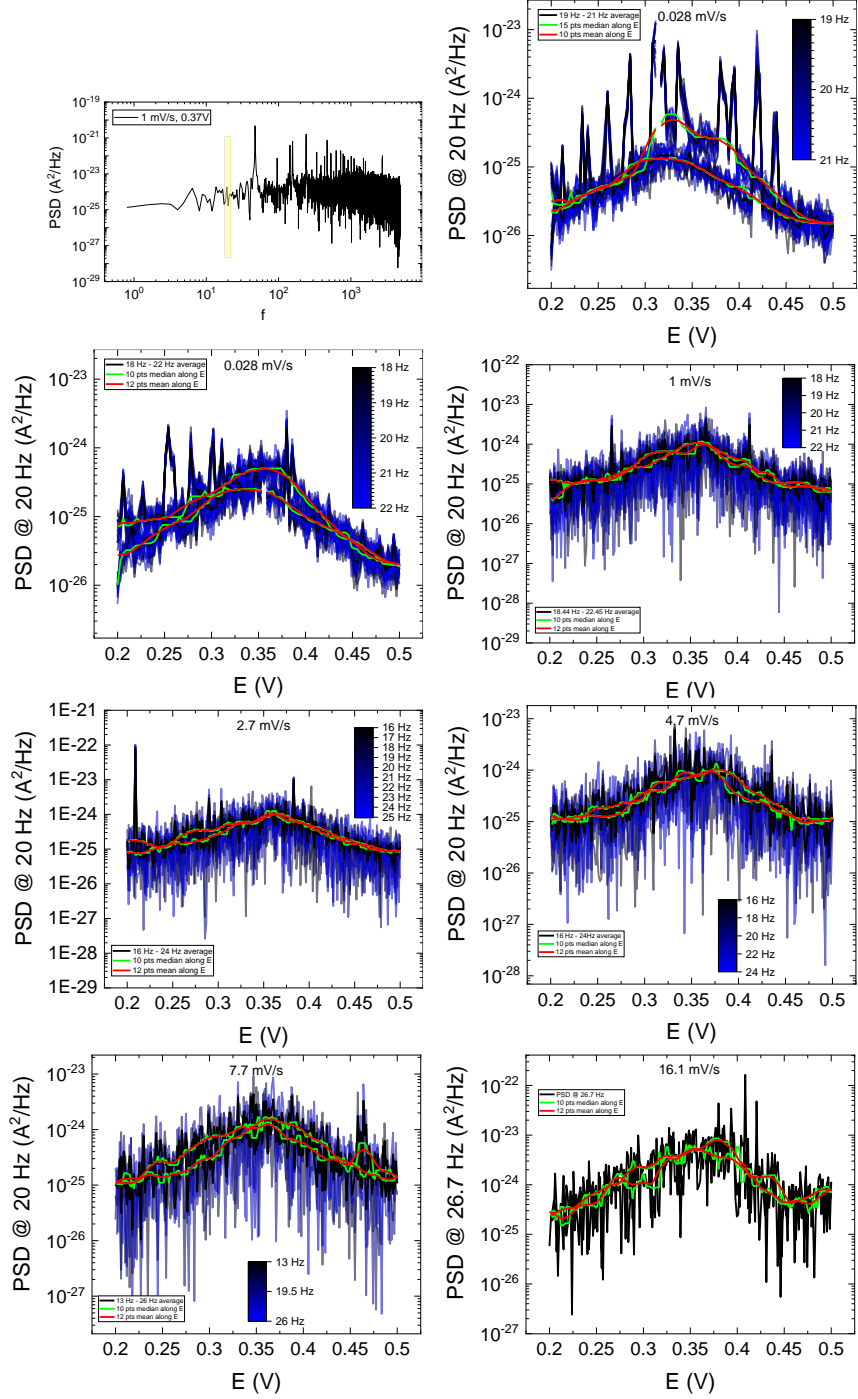


FIG. S9. Smoothing procedure used to obtain Figure 3 in the main text. The noise is taken at 20 Hz (yellow square on the spectrum), averaging with neighboring frequencies (blue lines, average in black). A rolling median (window $\approx 7\%$, green line) followed by an adjacent averaging (window $\approx 7\%$, red line) were used.

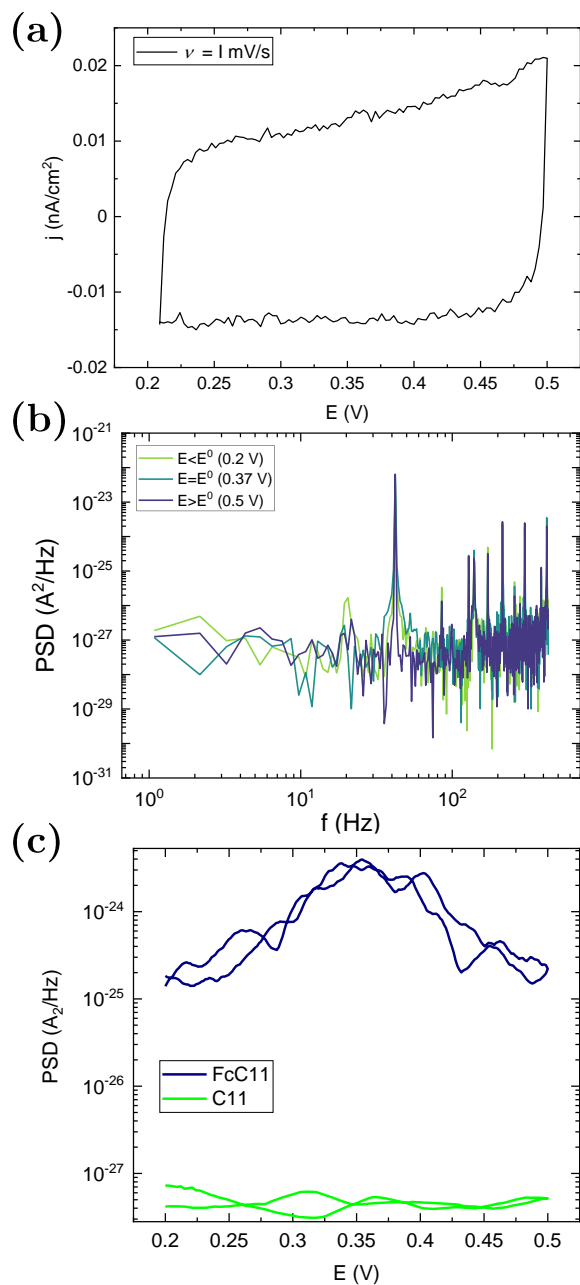


FIG. S10. (a) CV of a C₁₁SH SAM on gold. (b) PSD measured at 1 mV/s at $E < E^0$, $E \approx E^0$ and $E > E^0$. (c) PSD versus potential at 10 Hz, comparing C₁₁SH and FcC₁₁SH curves obtained at the same scanrate (1 mV/s).

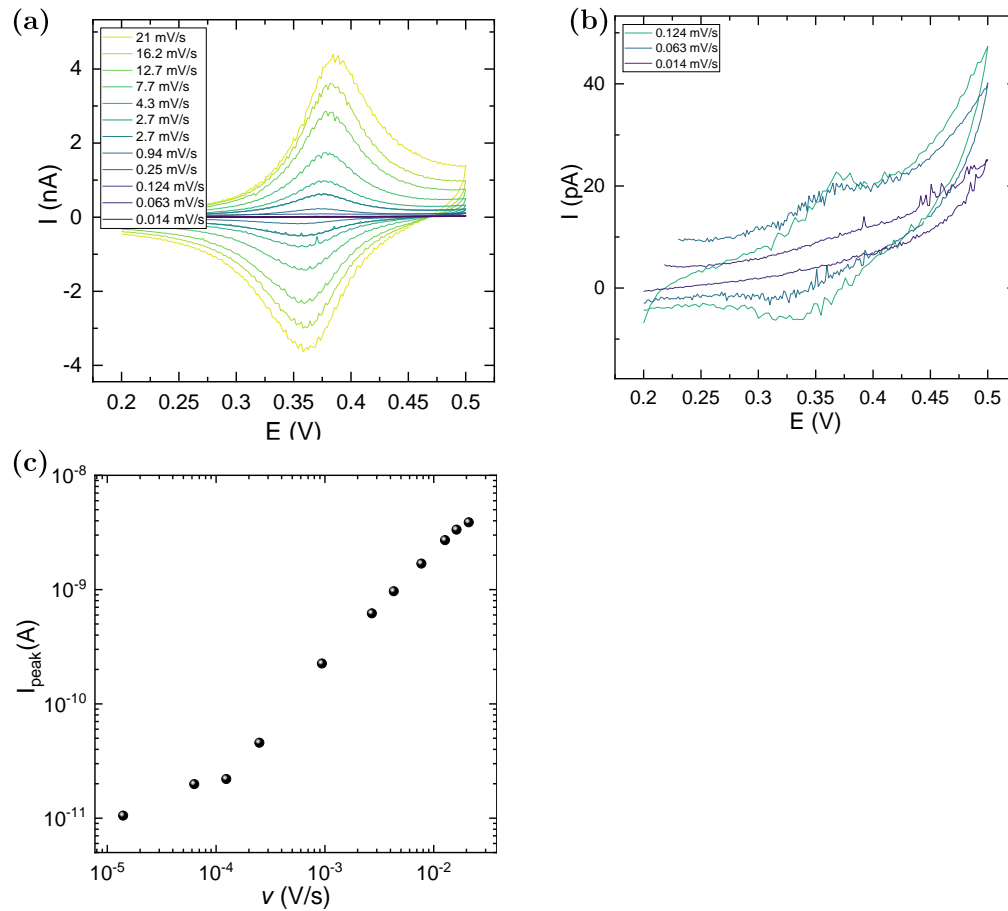


FIG. S11. Current CV (a) with zoomed data (b) corresponding to the data shown Figure 3 in the main paper. (c) shows the dependency of the current with the scan rate. From the area of the oxidation peak on the current CV, we estimate the number of molecules $N \approx 7.5 \times 10^{10}$.

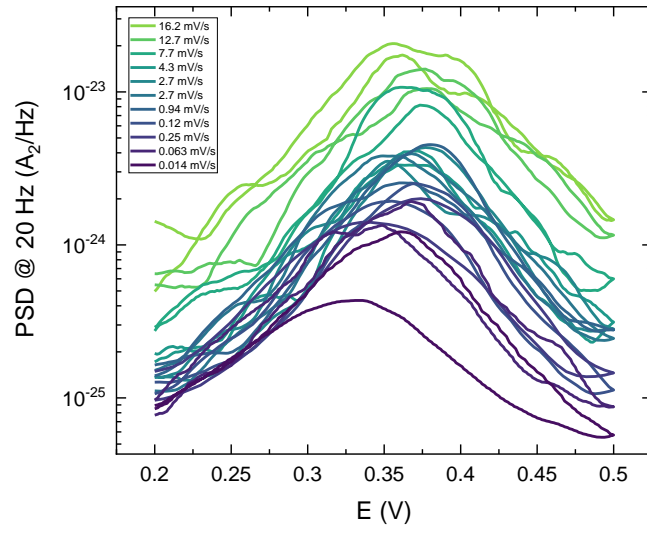


FIG. S12. PSD of the current versus E obtained at different ν , at $f \approx 20$ Hz, corresponding to the data shown in the main paper Figure 3.

FLUCTUATIONS OF k_0

Based on the simple Butler-Volmer description of the electron transfer, we assume a lognormal distribution of the electronic coupling H such as $k_0 \propto H^2$. H is taken so that the average value of $6.3 \times 10^8 \text{ s}^{-1}$ for k_0 , with a σ from 0.1% to 10%, similar to what was observed in [8]. This leads to the following distributions of k_0 Figure S13, with associated noise for PSD Figure S14.

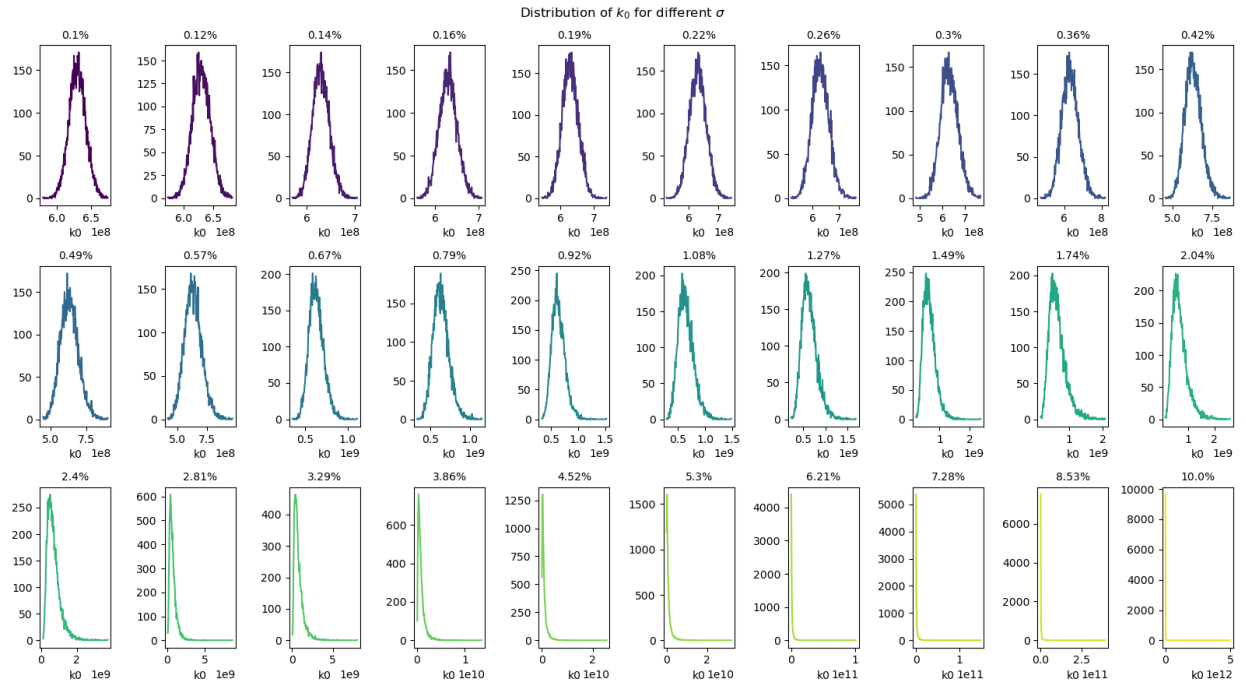


FIG. S13. Distribution of k_0 resulting from fluctuations of the electronic coupling (percentages indicated above each graph).

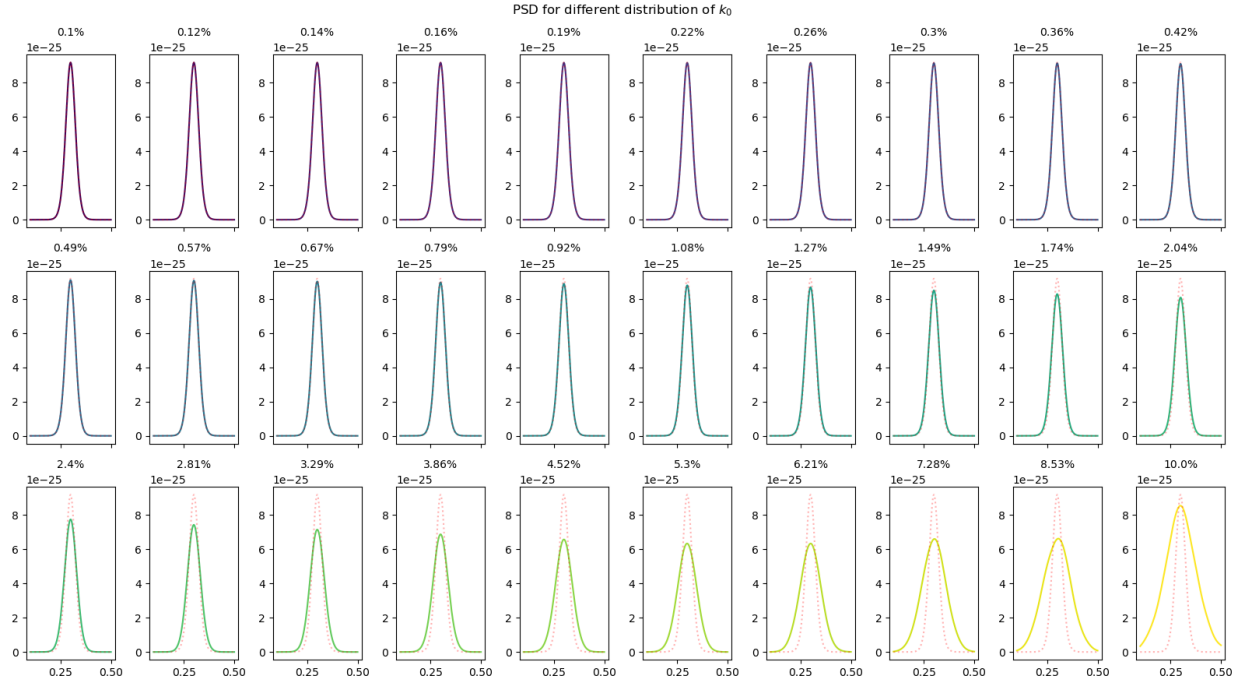


FIG. S14. PSD voltnoisograms resulting from fluctuations of the electronic coupling (percentages indicated above each graph). The dashed line is the PSD obtained with no fluctuations of k_0 .

IMPACT OF THE PERMITTIVITY OF WATER

Looking at the impact of the permittivity of water ε_{H_2O} through the electrostatic interactions φ such as defined by Eq. 12 allows to see its effect on current CV and PSD voltnoisograms. To this end, we carried out simulations with normal distributions of the intermolecular distance d with different standard deviations δd , such as done in [8]. The impact on current CV and noise voltnoisograms is estimated with their full width at half maximum (FWHM). One set was simulated with ε_{H_2O} (Figure S15), the other with ε_{SiO_2} (Figure S16), showing variations of few percent and tens of percent respectively in the FWHM for both current and PSD.

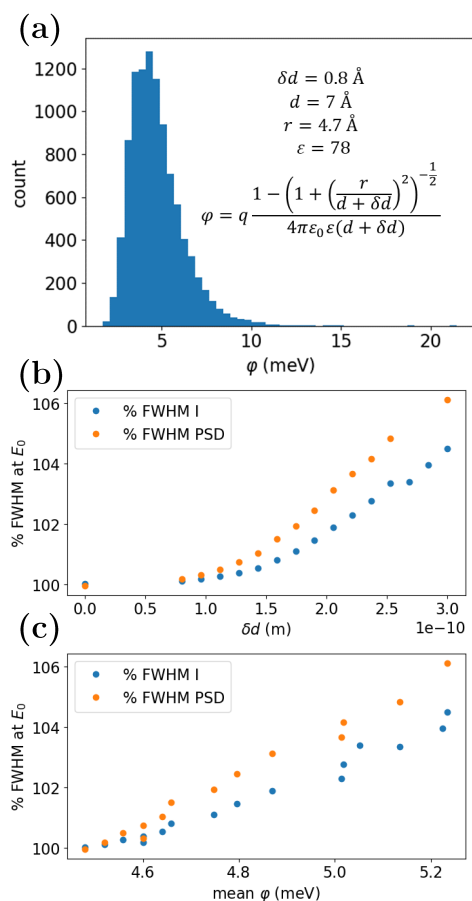


FIG. S15. (a) Distribution of φ corresponding to a normal distribution of d ($\delta d = 7 \text{ \AA}$ shown here) in water. Variation of the FWHM of CV and voltnoisogram versus (b) δd and the corresponding mean value of φ (c).

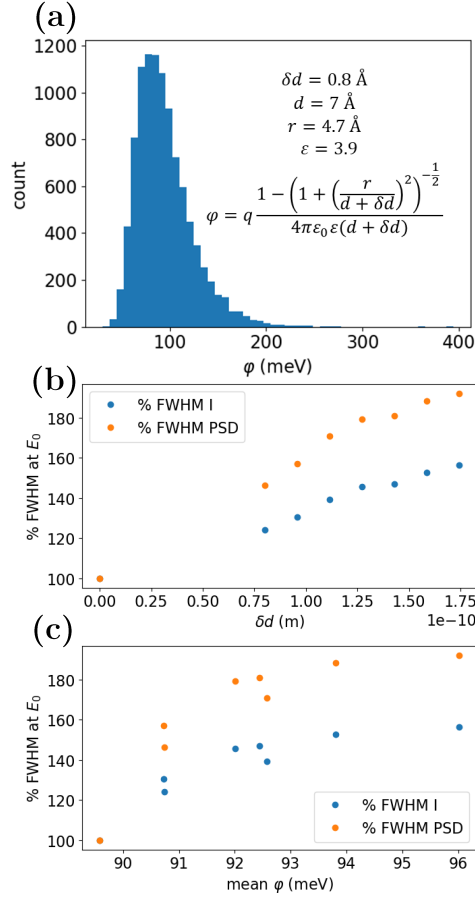


FIG. S16. (a) Distribution of φ corresponding to a normal distribution of d ($\delta d = 7 \text{ \AA}$ shown here) in silicon dioxide. Variation of the FWHM of CV and voltnoisogram versus (b) δd and the corresponding mean value of φ (c).

DISCUSSION ON THE DENOMINATION OF THE NOISE

We acknowledge that the denomination of the noise in the present study may be open for debate. The shot noise is most commonly measured in two-electrodes devices leading to the equation $S = 2qI$, with I the current flowing between the two electrodes and here $I = 0$ as a result of two currents canceling each other in this single electrode configuration. However, the original nature of the shot noise lies in the quantization of the electric charge and was previously understood as is by the electrochemists' community [9, 10], which is what motivates our proposal of “Electrochemical shot noise” for the noise in the present study.

-
- [1] E. Laviron, *Journal of Electroanalytical Chemistry and Interfacial Electrochemistry* , 10 (1979).
- [2] K.-C. Huang and R. J. White, *Journal of the American Chemical Society* **135**, 12808 (2013).
- [3] S. Westerlund and L. Ekstam, *IEEE Transactions on Dielectrics and Electrical Insulation* **1**, 826 (1994).
- [4] C. Wen, S. Zeng, K. Arstila, T. Sajavaara, Y. Zhu, Z. Zhang, and S.-L. Zhang, *ACS Sensors* **2**, 300 (2017).
- [5] N. Clément, S. Pleutin, D. Guérin, and D. Vuillaume, *Physical Review B* **82**, 035404 (2010).
- [6] K. Prabha and H. S. Jayanna, *Open Journal of Polymer Chemistry* **05**, 47 (2015).
- [7] N. E. Israeloff, *Physical Review B* **53**, R11913 (1996).
- [8] J. Trasobares, J. Rech, T. Jonckheere, T. Martin, O. Aleveque, E. Levillain, V. Diez-Cabanes, Y. Olivier, J. Cornil, J. P. Nys, R. Sivakumarasamy, K. Smaali, P. Leclere, A. Fujiwara, D. Théron, D. Vuillaume, and N. Clément, *Nano Letters* **17**, 3215 (2017).
- [9] W. Schottky, *Annalen der Physik* **362**, 541 (1918).
- [10] P. S. Singh and S. G. Lemay, *Analytical Chemistry* **88**, 5017 (2016).